JACS
JOURNAL OF THE AMERICAN CHEMICAL SOCIETY
Article
pubs.acs.org/JACS

# Engineering a Rigid Protein Tunnel for Biomolecular Detection

Mohammad M. Mohammad,[†] Raghuvaran Iyer,[‡] Khalil R. Howard,[§] Mark P. McPike,[∥] Philip N. Borer,[‡,§,∥] and Liviu Movileanu*[,†,§,⊥]

[†]Department of Physics, Syracuse University, 201 Physics Building, Syracuse, New York 13244-1130, United States
[‡]Department of Chemistry, Syracuse University, Syracuse, New York 13244-4100, United States
[§]Structural Biology, Biochemistry, and Biophysics Program, Syracuse University, 111 College Place, Syracuse, New York 13244-4100, United States
[∥]AptaMatrix, Inc., 100 Intrepid Lane Suite 1, Syracuse, New York 13205, United States
[⊥]The Syracuse Biomaterials Institute, Syracuse University, 121 Link Hall, Syracuse, New York 13244, United States

Supporting Information

**ABSTRACT:** One intimidating challenge in protein nanopore-based technologies is designing robust protein scaffolds that remain functionally intact under a broad spectrum of detection conditions. Here, we show that an extensively engineered bacterial ferric hydroxamate uptake component A (FhuA), a $\beta$-barrel membrane protein, functions as a robust protein tunnel for the sampling of biomolecular events. The key implementation in this work was the coupling of direct genetic engineering with a refolding approach to produce an unusually stable protein nanopore. More importantly, this nanostructure maintained its stability under many experimental circumstances, some of which, including low ion concentration and highly acidic aqueous phase, are normally employed to gate, destabilize, or unfold $\beta$-barrel membrane proteins. To demonstrate these advantageous traits, we show that the engineered FhuA-based protein nanopore functioned as a sensing element for examining the proteolytic activity of an enzyme at highly acidic pH and for determining the kinetics of protein−DNA aptamer interactions at physiological salt concentration.

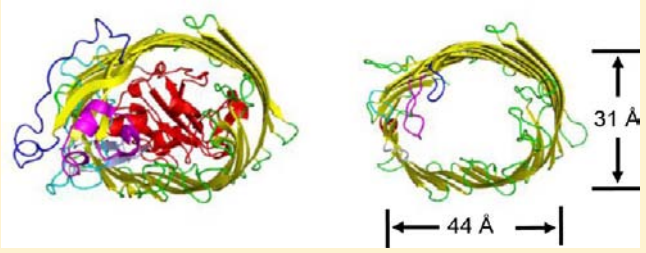


## 1. INTRODUCTION

Protein-based nanosensors represent an emergent alternative to current analytical devices in biomedical molecular diagnosis, because of their enhanced selectivity, specificity, and versatility of the protein receptor−ligand recognition.[1] Significant progress in protein engineering enabled the design, synthesis, and purification of protein nanopores customized to execute numerous complex tasks.[2−6] The underlying detection principle relies on current modulation as a result of individual biomolecular binding events between a specific analyte and a single nanopore.[2,3,7] Currently, the engineering of biological nanopores is focused on pore-forming toxins and bacterial outer membrane proteins, because their robust $\beta$-barrel structure makes them the convenient choice for developing sensing technologies.[6] The major benefits of using protein nanopores include knowledge of their accurate structure at atomic resolution, the ability to implement functional groups at strategic positions within their interior, and great prospects for parallelization and integration into nanofluidic devices. Despite these advantageous features, one persistent limitation is the lack of a methodology for preparing stiff protein scaffolds that maintain their functionality under a wide spectrum of environmental conditions.

Here, we show that this challenge may be addressed using an extensively engineered bacterial ferric hydroxamate uptake component A (FhuA), a monomeric outer membrane protein of *E. coli*.[8,9] We demonstrate that a heavily redesigned FhuA protein readily forms a robust protein tunnel in a synthetic bilayer, with a unitary conductance of ~3.9 nS. More importantly, the engineered FhuA protein nanopore maintains its gating-free, open-state electrical signature for long periods under an unusually broad range of conditions. We define a stable protein nanopore as an engineered transmembrane protein that exhibits a pore-forming ability and lacks large-amplitude current fluctuations under the examined conditions. FhuA is a 714-residue protein composed of 22 antiparallel $\beta$ strands (Figure 1a).[8,9] The $\beta$ barrel of the FhuA protein contains an N-terminal 160-residue cork domain. The $\beta$ strands are linked by eleven loops on the extracellular side and ten short turns on the periplasmic side (Figure 1a). A distinctive feature of this protein is its remarkable variety of functionalities, including the dual task of transporter and receptor. The primary role of FhuA is to facilitate the energy-driven, high-affinity $Fe^{3+}$ uptake complexed by the siderophore ferrichrome,[10] yet its transporter role further extends to antibiotics, such as albomycin[11] and rifamycin.[12] In addition, the FhuA protein functions as a receptor for the colicin M toxin and a number of bateriophages, including T1, T5, and $\phi$80.[13]

Prior studies that employed various loop deletions and cork removal of the FhuA protein indicated the potential to derive an

**Received:** May 5, 2012
**Published:** May 12, 2012

   dx.doi.org/10.1021/ja3043646 | J. Am. Chem. Soc. 2012, 134, 9521−9531

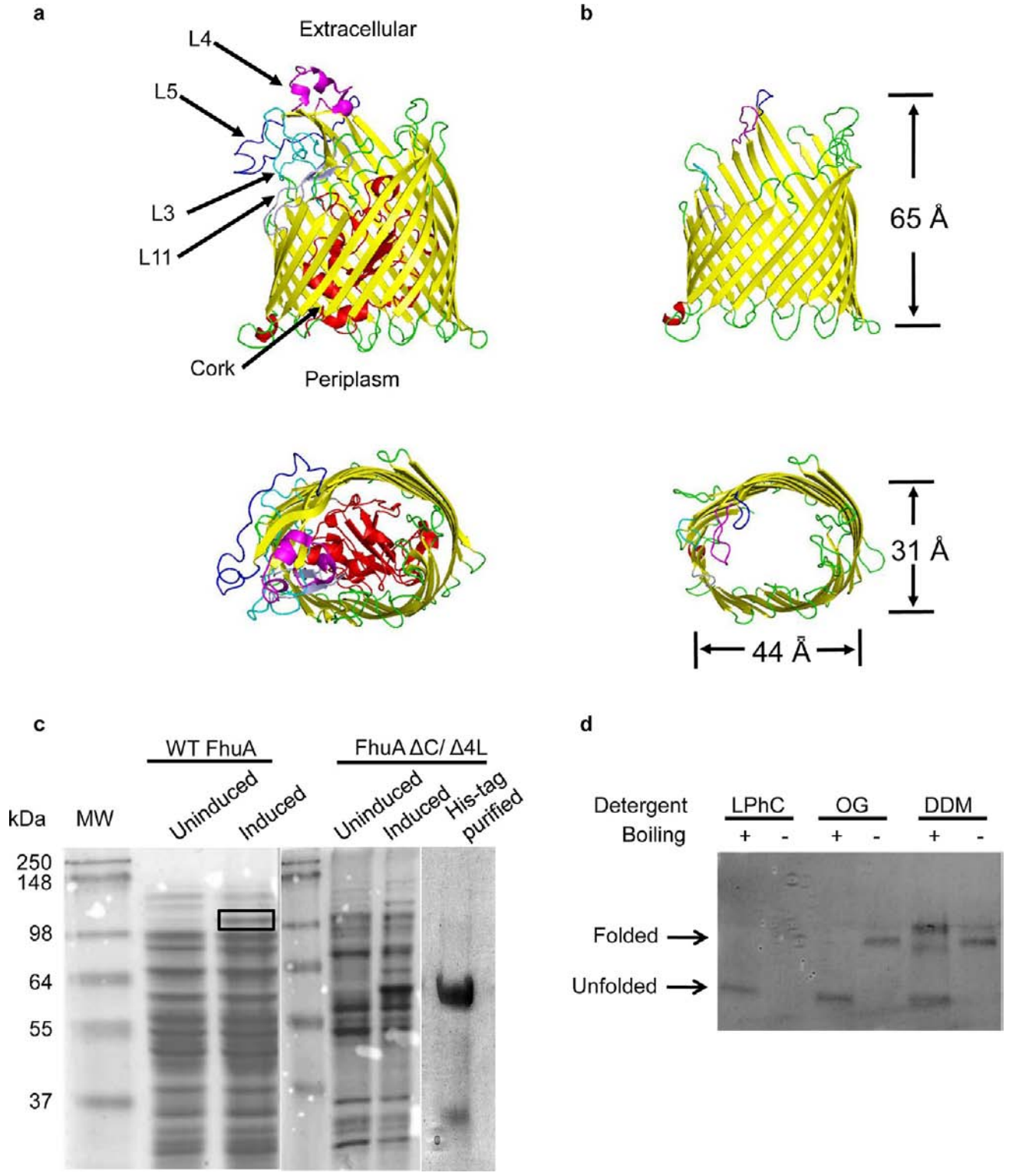


**Figure 1.** Coupling genetic engineering with a rapid-dilution refolding protocol to produce a functionally stable and robust protein nanopore. Panels a and b indicate the wild-type FhuA (WT-FhuA) and engineered FhuA ΔC/Δ4L proteins, respectively. The top and bottom panels show the side and extracellular views, respectively. The FhuA ΔC/Δ4L protein pore was designed by deleting loops L3 (cyan), L4 (magenta), L5 (blue), and L11 (light blue) and the first 160 amino acids (the cork domain, red) of the WT-FhuA protein. These large extracellular loops were replaced with peptide linker NSEGS (linkers have similar color to that of the deleted loops). (c) Coomassie blue-stained SDS-PAGE gel indicating the purified FhuA ΔC/Δ4L protein pore. Protein samples underwent heating up to 95 °C for 5 min before loading. MW stands for molecular weight standard. About 3 $\mu$g of purified FhuA ΔC/Δ4L protein was added, whereas the 36-kDa band was always copurified with the FhuA ΔC/Δ4L protein band and both were identified by his-tag stain. (d) Heat modifiability assay for the refolded FhuA ΔC/Δ4L protein nanopores.[18] Samples were loaded on the SDS-PAGE gel either with (+) or without (−) heating at 95 °C for 5 min. LPhC, OG, and DDM indicate 1-lauroyl-2-hydroxy-*sn*-glycero-3-phosphocholine, *n*-octyl-$\beta$-D-glucopyranoside, and *n*-dodecyl-$\beta$-D-maltopyranoside, respectively.


dx.doi.org/10.1021/ja3043646 | *J. Am. Chem. Soc.* 2012, 134, 9521−9531

open FhuA protein pore.[14,15] These early measurements employed multichannel currents at lower time resolution, precluding a systematic exploration of spontaneous gating of each engineered FhuA protein. Previously, we employed high-resolution, time-resolved single-channel electrical recordings and identified four large loops, L3, L4, L5, and L11, located on the extracellular side, which can fold back into the pore lumen, resulting in spontaneous gating of the pore (Figure 1a, b).[16] An FhuA protein lacking both the cork domain and the four extracellular loops mentioned above, FhuA ΔC/Δ4L, inserted into a synthetic planar lipid membrane and formed an open transmembrane pore, but with some caveats. The engineered FhuA ΔC/Δ4L protein was either extracted from native membranes or derived from inclusion bodies and then refolded following an on-column refolding protocol. In general, the membrane-extracted FhuA proteins undergo a laborious procedure with unsatisfactory yields. However, the major disadvantage of membrane-extracted and on-column refolded, inclusion body-derived FhuA ΔC/Δ4L protein nanopores was that they show long-lived spontaneous gating at applied transmembrane potentials greater than ∼50 mV.[16] In addition, the engineered FhuA ΔC/Δ4L protein nanopores derived by these approaches exhibited a broad distribution of the values of single-channel conductance, ranging from 2.5 to 6.5 nS.[16]

## 2. RESULTS AND DISCUSSION

In this work, we show that these limitations may be overcome by adopting a simple rapid-dilution protocol[17] and employing proteins advantageously produced in the inclusion bodies.[18] We diluted the denatured, affinity-purified FhuA ΔC/Δ4L protein in buffer solution that contained *n*-dodecyl-*β*-D-maltopyranoside (DDM), *n*-octyl-*β*-D-glucopyranoside (OG), or 1-lauroyl-2-hydroxy-*sn*-glycero-3-phosphocholine (LPhC) detergent (Supporting Information). The engineered FhuA ΔC/Δ4L proteins exhibited heat modifiability in their electrophoretic mobility on SDS-PAGE gel, suggesting that they acquired properties of refolded *β*-barrel proteins (Figure 1c, d).[18] Similar findings were not obtained using other detergents, such as Zwittergent 3-14 and *N*,*N*-dimethyldodecylamine-*N*-oxide (LDAO).

We used high-resolution, single-channel electrical recordings to examine the properties of the engineered FhuA ΔC/Δ4L protein nanopore. Addition of detergent into the chamber, up to ∼0.01% LPhC, OG, or DDM, did not influence the stability or the insulating nature of the synthetic bilayer (Figure 2a). The *cis* chamber was grounded so that a positive current (upward deflection) represents positive charge moving from the *trans* to *cis* chamber. Our initial tests indicated that the engineered FhuA ΔC/Δ4L protein nanopores had a closely similar unitary conductance regardless of the detergents used in the refolding protocol (Supporting Information, Table S1). Here, we present the single-channel data obtained with DDM-refolded FhuA ΔC/Δ4L protein. Upon its addition to the *cis* chamber, the engineered FhuA ΔC/Δ4L protein nanopore showed a pore-forming activity, as evidenced by the discrete, stepwise increase in membrane conductance (Figure 2b). The unitary current, in 1 M KCl, 10 mM potassium phosphate, pH 7.4, was 156 ± 21 pA at an applied potential of +40 mV, which corresponded to a single-channel conductance of ∼3.9 ± 0.5 nS ($n$ = 92, Figure 2b, Supporting Information, Table S1). Spontaneous insertions of the FhuA ΔC/Δ4L protein nanopores required neither an osmotic gradient nor supplementary preparative steps, such as reconstitution into proteoliposomes. In Figure 2c, we show a representative trace recorded with FhuA ΔC/Δ4L at 120 mV. Furthermore, the FhuA ΔC/Δ4L protein nanopore maintained its open state for long periods, in the range of several tens of minutes through hours. The distribution of the values of unitary conductance showed a peak centered at ∼3.9 nS (Figure 2d). According to the X-ray crystal structure of the native FhuA protein, the cross-sectional area of the engineered cork-free FhuA protein nanopore is elliptical and has the internal average dimensions of 2.6 × 3.9 nm (including the side chains of the residues) (Figure 1b).[8,9] Single-channel recordings of FhuA ΔC/Δ4L in the presence of 40-kDa dextran polymer, added symmetrically to the *cis* and *trans* chambers, suggested that the average cross-sectional diameter of the FhuA ΔC/Δ4L protein nanopore is ∼2.2 nm. This result was obtained by measuring the contribution of the access resistance to the total resistance of the nanopore. The effective diameter of the nanopore was calculated using the simplified assumption that FhuA ΔC/Δ4L is a nonselective cylinder at 1 M KCl (Supporting Information, Figure S2).[19]

To reliably measure the nanopore conductance, we derived the slope from the current versus voltage plot, which gives 3.9 ± 0.2 nS in 1 M KCl, 10 mM potassium phosphate, pH 7.4 (Figure 2e). The data was obtained from at least five distinct experiments and using two different protein preparations. In addition, we performed single-channel electrical recordings with a single FhuA ΔC/Δ4L protein nanopore under a voltage ramp, using the same experimental conditions (Figure 2f). We found that the slopes of the fitted curve provided values of ∼3.6 nS and ∼7.7 nS for a single nanopore and two nanopores, respectively. The voltage-ramp scanning showed that the FhuA ΔC/Δ4L protein nanopores exhibited a gating-free, open-state signature at applied transmembrane potentials in the range between −140 and +140 mV (Figure 2f). FhuA ΔC/Δ4L inserted into a planar lipid bilayer as a monomer and in a single orientation (Supporting Information, Figure S3).

Critically important for this work and future applications, the engineered FhuA ΔC/Δ4L protein nanopore maintained its open state under a broad range of conditions. The gating-free signature of the single-channel current was consistently observed at highly acidic pH values (Supporting Information, Figure S4) and over a wide range of KCl concentrations, between 20 mM and 4 M (Supporting Information, Figure S5). To illustrate this fundamental asset of FhuA ΔC/Δ4L, we provide, in Figure 3, a side-by-side comparison between the electrical signatures of the commonly used protein nanopore, the staphylococcal *α*-hemolysin (*α*HL), and FhuA ΔC/Δ4L under low salt concentration and highly acidic pH conditions. The top panels indicate single-channel (Figure 3a, *α*HL; Figure 3b, FhuA ΔC/Δ4L) and macroscopic (multichannel survival curve; Figure 3c) current recordings collected at 200 mM KCl, 10 mM potassium phosphate, pH 7.4. Clearly, FhuA ΔC/Δ4L exhibited a better signal-to-noise ratio than *α*HL at physiological salt concentration. *α*HL showed frequent and large-amplitude current spikes, similar to the cases of other studies,[20] which were absent in FhuA ΔC/Δ4L. Independently recorded multichannel survival curves also confirmed superior stability of the open-state current of FhuA ΔC/Δ4L as compared to *α*HL (Figure 3c). To our knowledge, all stochastic sensing studies employing *α*HL were carried out at salt concentrations greater than the physiological conditions (>200 mM salt).[3,4,6,21−23] It is worth noting that even the newly engineered multimeric-protein nanopores, MspA[24,25] and membrane-adapted phi29 motor protein,[26] were also used in buffers with an ionic strength greater than those of physiological conditions.

We pursued a similar comparison between *α*HL and FhuA ΔC/Δ4L at 1 M NaCl, 10 mM phosphate-citrate, pH 3.5. Under these conditions, the distinction between *α*HL and FhuA ΔC/Δ4L was amplified owing to the large-amplitude and long-lived current blockades observed with *α*HL at highly acidic pH (Figure 3d, *α*HL;

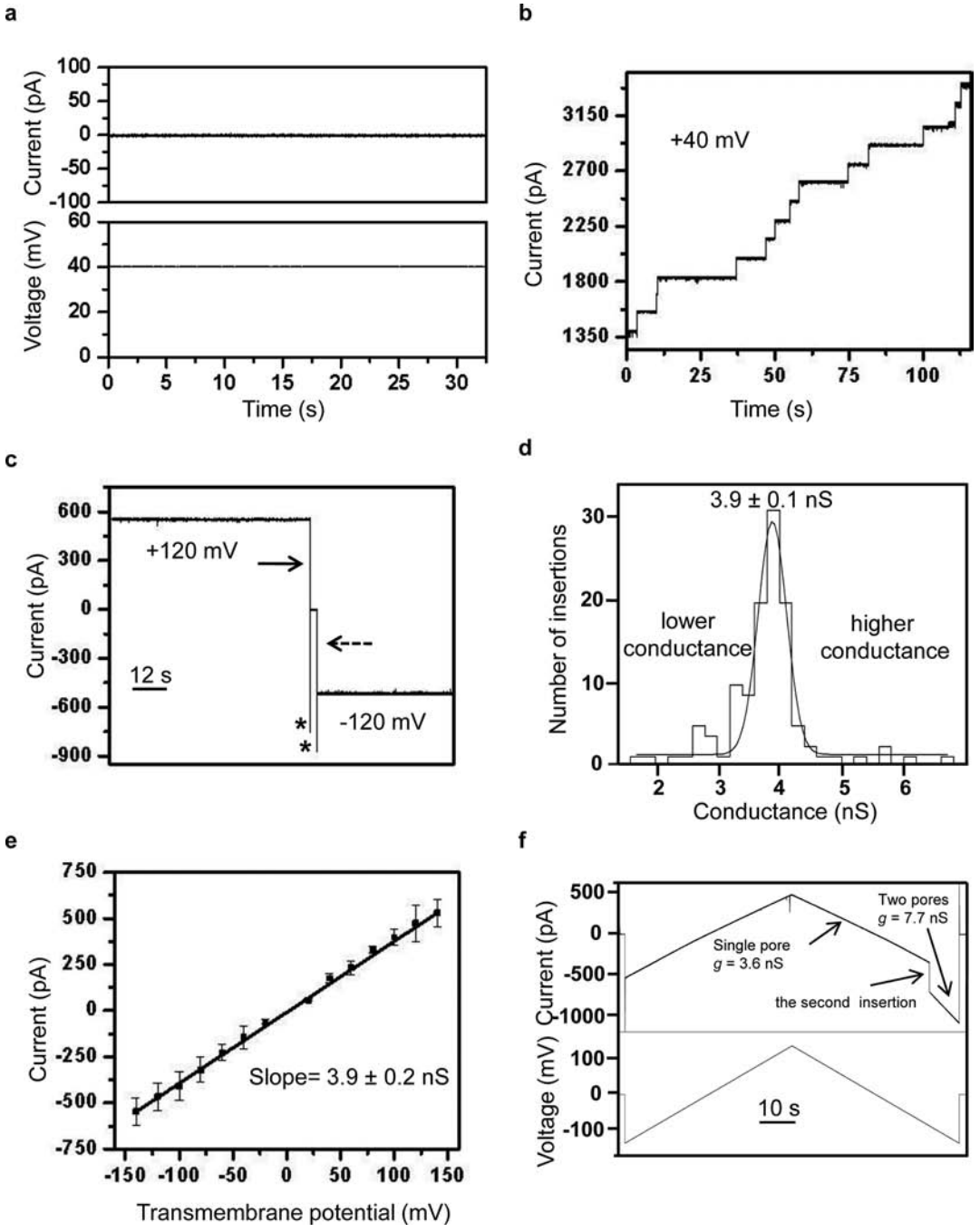


**Figure 2.** Spontaneous insertion of the engineered FhuA ΔC/Δ4L protein nanopore into a lipid bilayer. (a) The electrical signature of the synthetic bilayer formed on a ~50 $\mu$m aperture in 1 M KCl, 10 mM potassium phosphate, pH 7.4, and in the presence of 0.01% DDM. The applied transmembrane potential was +40 mV. (b) Insertions of single channels in the bilayer after the addition of 150 ng of refolded FhuA ΔC/Δ4L protein at an applied transmembrane potential of +40 mV. The reproducibility of this multiple single-channel insertion measurement was tested over 60 distinct experiments. (c) Single-channel recording at an applied potential of +120 mV and −120 mV. Turning off (the solid arrow) and turning on (dashed arrow) the applied transmembrane potential resulted in a current deflection (asterisks). (d) Standard histogram of the distribution of single-channel conductance values of the FhuA ΔC/Δ4L protein nanopores at an applied transmembrane potential of +40 mV. (e) Relationship between current and voltage of single protein nanopores ($I/V$ curve). Error bars are determined from at least 5 distinct experiments. (f) Voltage ramps of one and two protein nanopores. The speed of voltage ramping was 1.4 mV $s^{-1}$. The conductance, $g$, was 3.6 and 7.7, for one and two nanopores, respectively. Data was obtained with DDM, except in part c (OG). The electrical traces were low-pass Bessel filtered at 2 kHz, except in part f, at 0.1 kHz, to eliminate the noise from the amplifier during the application of the voltage ramp.

Figure 3e, FhuA ΔC/Δ4L; multichannel survival curve; Figure 3f), similar to previous studies.[27,28] These data indicate the absence of large-amplitude current blockades in recordings with FhuA ΔC/Δ4L at a transmembrane potential of +100 mV, which is advantageous for single-molecule detection experiments under the above-mentioned conditions. However, at low salt concentration, the low-amplitude current fluctuations were on the same order of magnitude for both nanopores, but these fluctuations were greater in the case of FhuA ΔC/Δ4L at acidic pH, as evidenced in the noise spectra analysis (Figure 3g and h). We judge that these low-amplitude current


dx.doi.org/10.1021/ja3043646 | J. Am. Chem. Soc. 2012, 134, 9521−9531

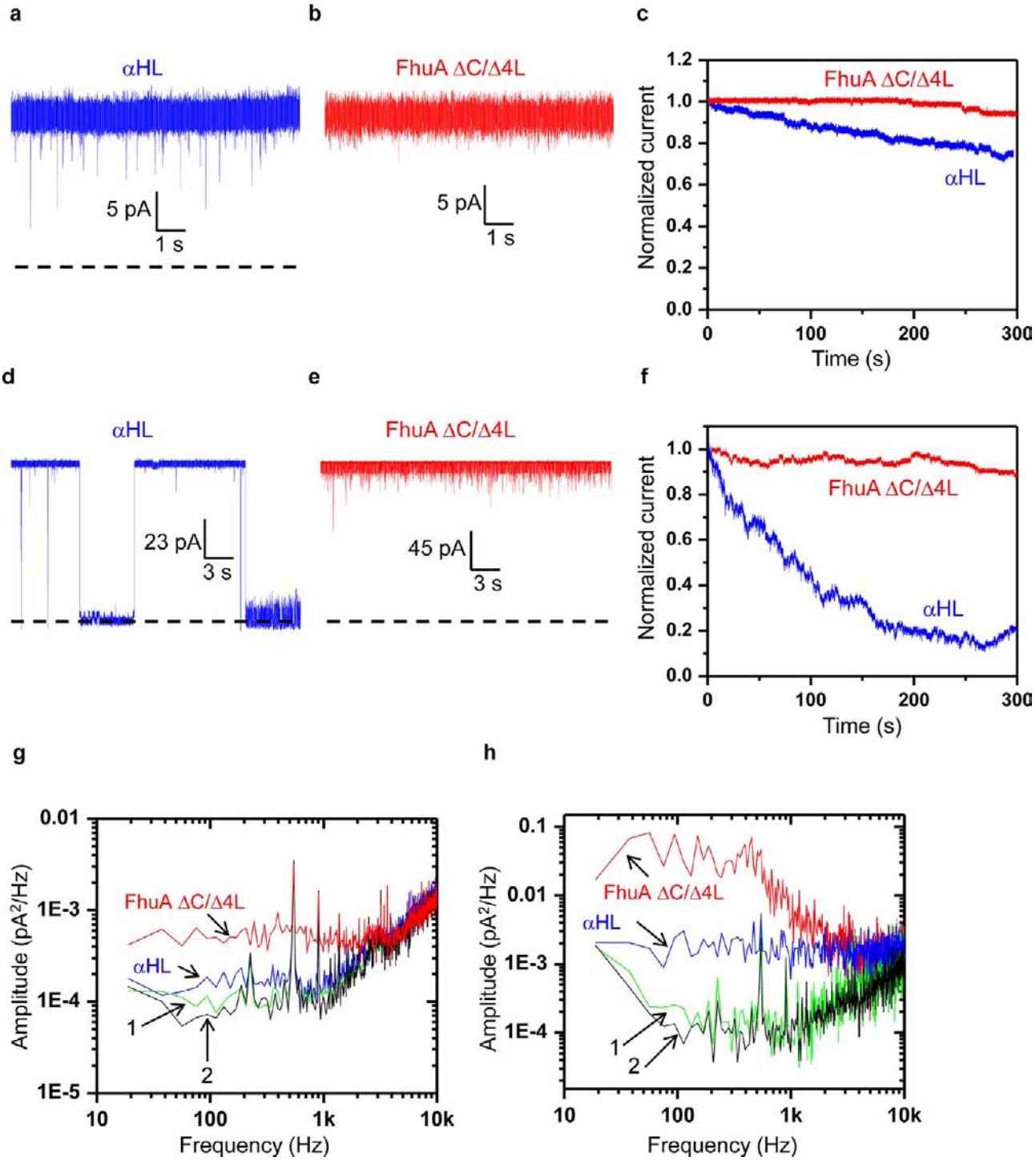


**Figure 3.** Comparison of the electrical signatures between staphylococcal $\alpha$-hemolysin ($\alpha$HL) and FhuA ΔC/Δ4L. This figure shows single-channel electrical recordings with the open-state current of the wild-type $\alpha$HL nanopore (a) and the engineered FhuA ΔC/Δ4L nanopore (b) at low physiological salt concentration (200 mM KCl, 10 mM potassium phosphate, pH 7.4) and at an applied transmembrane potential of +100 mV. (c) Macroscopic current recordings for the exploration of the instability of the open-state current of the engineered FhuA ΔC/Δ4L and $\alpha$HL protein pores; experimental conditions are as in parts a and b. Shown are single-channel electrical recordings for the $\alpha$HL nanopore (d) and the engineered FhuA ΔC/Δ4L nanopore (e) in 1 M NaCl, 10 mM phosphate-citrate buffer, pH 3.5, at an applied transmembrane potential of +100 mV. (f) Macroscopic current recordings for the exploration of the instability of the open-state current of the engineered FhuA ΔC/Δ4L and $\alpha$HL protein pores; experimental conditions are as in parts a and b. All electrical traces were low-pass Bessel filtered at 2 kHz. Noise spectral density acquired with FhuA ΔC/Δ4L and $\alpha$HL (g and h). (g) Data are collected at +100 mV for the two nanopores in salt conditions as in parts a and b. The five seconds of traces a and b were used for the analysis. Noise spectral densities taken at 0 mV for FhuA ΔC/Δ4L and $\alpha$HL nanopores are marked by 1 and 2, respectively. (h) Noise spectral density collected at +100 mV with the two nanopores under the conditions of parts d and e of pH. 5-s duration of traces from parts d and e was used for the analysis. Noise spectral densities taken at 0 mV for FhuA ΔC/Δ4L and $\alpha$HL nanopores are marked by 1 and 2, respectively. All current measurements were performed at a sampling rate of 50 kHz with an internal low-pass Bessel filter set at 10 kHz, and portions of traces were analyzed with no additional filtering. Dashed lines represent zero current. Macroscopic current recordings were carried out with ~32 FhuA ΔC/Δ4L, ~35 $\alpha$HL nanopores in part c, and ~55 FhuA ΔC/Δ4L, ~60 $\alpha$HL nanopores in part f.


dx.doi.org/10.1021/ja3043646 | J. Am. Chem. Soc. 2012, 134, 9521−9531

fluctuations are due to some conformational and structural changes in the remaining extracellular loops. Similar to αHL,[29] FhuA ΔC/Δ4L was open at pH 11.6 when the applied transmembrane potential was +80 mV (Supporting Information, Figure S4). The voltage dependence of the multichannel survival curves revealed a highly stable open-state current of FhuA ΔC/Δ4L at low salt concentration and at negative transmembrane potentials, and a significantly stable FhuA ΔC/Δ4L at low pH condition as compared to αHL (Supporting Information, Figure S6; Table S2).

We also noted that the engineered FhuA ΔC/Δ4L protein nanopore maintained its stable open state for long periods at temperatures up to 65 °C (Supporting Information, Figure S5), confirming the robustness of the β-barrel structure.[30] The crystal structure of the native FhuA protein shows numerous pools of negatively charged residues within the pore lumen.[8,9] In agreement with this observation, we found that the FhuA ΔC/Δ4L protein nanopore exhibits the permeability ratio $P_K/P_{Cl}$ of 5.5 ± 1.7 under asymmetric conditions of 20 mM KCl/200 mM KCl (Supporting Information, Figure S7).

To illustrate these unique characteristics, we show three immediate examples of applications for the engineered FhuA ΔC/Δ4L protein in the single-molecule detection of biomolecular events, such as protein−protein and protein−nucleic acid interactions. In the first example, we demonstrate that this protein nanopore functions as a sensing element to discriminate among similar folded protein domains fused to positively charged polypeptides of varying lengths. The target protein was the small, globular 110-residue RNAase barnase fused to the unstructured N-terminal part of the $pb_2$ precytochrome.[31] We used three $pb_2$-Ba proteins of varying length and similar electric charge density of the $pb_2$ presequence (Supporting Information, **Table S3**).[31,32] Thus, the engineered protein analytes were $pb_2$(35)-Ba, $pb_2$(65)-Ba, and $pb_2$(95)-Ba with leading positively charged presequences of 35, 65, and 95 residues, respectively.

We first executed single-channel recordings with the FhuA ΔC/Δ4L protein nanopore in the presence of 200 nM $pb_2$-Ba added to the *trans* side of the bilayer. At a transmembrane potential of +80 mV and in 1 M KCl, 10 mM potassium phosphate, pH 7.4, all $pb_2$-Ba produced short-lived current blockades with an average dwell time of 0.20 ± 0.08 ms ($n$ = 3), but each featured distinct association rate constants (Supporting Information, Table S3, Figure S8). Different association rate constants derived with $pb_2^-$Ba proteins of varying presequence length indicated that their interaction with the protein nanopore is strongly dependent on the leading polypeptide arm (Supporting Information, Table S3). We interpret that the current blockades resulted from the direct interaction between the positively charged $pb_2$ arm and the negatively charged interior of the nanopore. A large folded protein domain, such as bovine serum albumin (BSA) did not produce single-channel current blockades when added to the *trans* side of the chamber (Supporting Information, Figure S9).

We performed the nanopore sensing detection at 20 mM KCl, in which the strength of the electrostatic interactions between the $pb_2$-Ba proteins and the FhuA ΔC/Δ4L nanopore is amplified. A low closure rate ($<3 \times 10^{-3}$ $s^{-1}$) of the macroscopic current was noticed with the FhuA ΔC/Δ4L protein nanopore when 100 nM $pb_2$(35)-Ba was added to the *trans* side of the chamber. In contrast, a rapid decay of the macroscopic current was recorded with $pb_2$(95)-Ba with a rate constant of $(28 \pm 9) \times 10^{-3}$ $s^{-1}$ ($n$ = 4). The residual currents found with $pb_2$(35)-Ba, $pb_2$(65)-Ba, and $pb_2$(95)-Ba were 0.72 ± 0.18, 0.55 ± 0.17, and 0.25 ± 0.12, respectively (Figure 4b, Supporting Information, Table S3). This result is in accord with the single-channel recording data that established an increasing rate constant of association with an increase in the length of the $pb_2$ presequence (Supporting Information, Figure S8 and Figure S10). Distinct interactions of FhuA ΔC/Δ4L with $pb_2$-Ba proteins of varying $pb_2$ length indicate that the $pb_2$ arm partitions into the nanopore lumen.

In the second example, we show that the engineered FhuA ΔC/Δ4L nanopore functions as a sensing element for the digestion of the serum immunoglobulin (IgG) protein at highly acidic pH. αHL nanopore has been used in examining the proteolytic digestion, but not at low pH conditions.[33] The pepsin protease has been previously investigated in its production of antigen-binding fragments (Fab) by digesting the Fc part of IgG at pH 1.5−4 under optimized conditions.[34] We used experimental conditions in which pepsin digested IgG completely (Supporting Information, Figure S11; Supporting Information, Tables S4 and S5). The underlying principle of nanopore-based detection is that the IgG fragments are detected upon pepsin digestion (Figure 4c). We further tracked the pepsin activity using time-course digestion of IgG under optimized conditions of 1 M NaCl, 10 mM phosphate-citrate, pH 3.9 (Figure 4d), so we could compare this activity to our single-channel trace signature. The nanopore-based diagnosis of the digestion activity is illustrated in Figure 4e, f. The FhuA ΔC/Δ4L nanopore is stable in the digestion buffer (Figure 4e, trace 1). The addition of pepsin to the *trans* side of the chamber did not produce significant change in the current recordings (Figure 4e, trace 2), presumably due to a large size of the enzyme as compared to the *trans* opening of the nanopore. In contrast, the presence of IgG in the chamber produced transient current blockades with an event frequency $f$ = 30 ± 8 $s^{-1}$ ($n$ = 3, Figure 4e, trace 3). Remarkably, the addition of pepsin ($t$ = 5 min) resulted in a drastic decrease of the event frequency ($f$ = 5 ± 2 $s^{-1}$ at $t$ = 10 min) (Figure 4e, trace 4). As expected, the fragments resulting from IgG digestion produced numerous transient current blockades, with an increased frequency ($f$ = 10 ± 2 $s^{-1}$ at $t$ = 70 min) (Figure 4e, trace 5). Time-course analysis of the frequency of the transient current blockades revealed important details about the digestion reaction (Figure 4f).

The frequency of the transient current blockades dropped ∼52% at $t$ = 0.5 min of the reaction and ∼70% at $t$ = 1 min. Interestingly, pepsin did not digest a significant amount of IgG at $t$ = 0.5 and digested only ∼5% of IgG at $t$ = 1 min (Figure 4d). We attribute these observations to the binding of pepsin to IgG, which reduced the frequency of the transient current blockades (Figure 4c). One obvious question of these single-channel results is why the event frequency after pepsin digestion never recovers to the initial value recorded before the onset of digestion. An immediate interpretation is that most resulting fragments have low molecular mass (Supporting Information, Tables S4 and S5) and, therefore can traverse the nanopore with very short transit times, precluding their observation. Other fragments do not partition into the nanopore interior due to a number of reasons, such as the charge distribution, the solution structure, or the hydrophobicity of the polypeptide chain of the fragments. Again, the 75-min duration of the nanopore experiment indicates that the FhuA ΔC/Δ4L bilayer system is stable for long periods under this highly acidic condition.

In the third example, we examined the kinetics of NCp7−DNA aptamer interactions through titration experiments using the FhuA ΔC/Δ4L nanopore at low physiological salt concentration. The major role of the 55-residue nucleocapsid (NC) domain of gag and gag-pol polyproteins in the HIV-1 infection cycle is to select the viral genomic RNA for packaging.[35,36] The mature NCp7 protein also has high affinity and specificity for the unpaired bases of RNA stem-loops in the packaging domain of genomic RNA at physiological salt concentrations.[37,38] The basic idea of nanopore-based

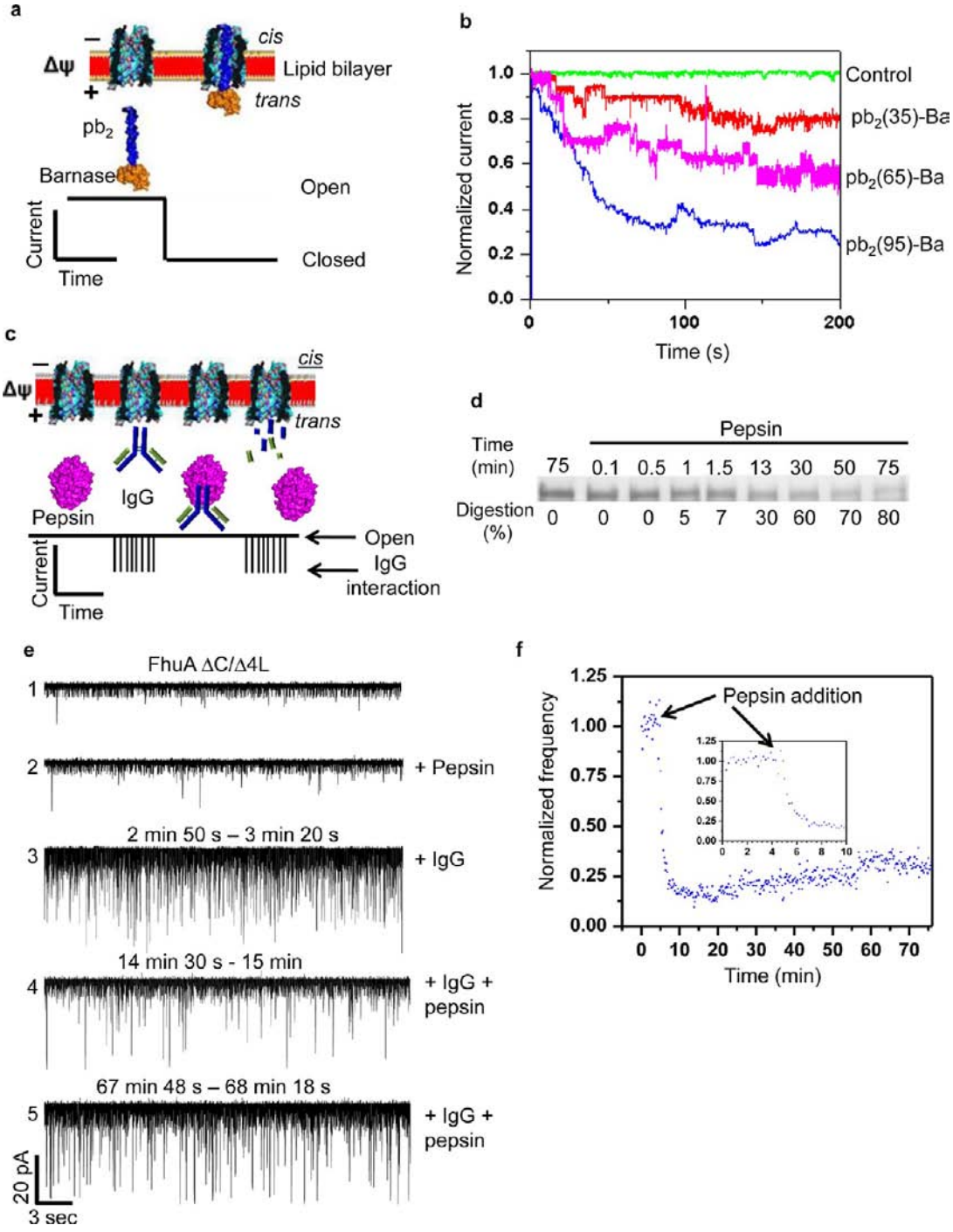


**Figure 4.** Applications for engineered FhuA ΔC/Δ4L protein nanopore in the single-molecule detection of proteins. The engineered FhuA ΔC/Δ4L protein nanopore was used as a single-molecule probe for inspecting folded protein domains fused to leading polypeptides of varying length (a and b) and real-time assay of enzymatic digestion (c–f). (a) Cartoon presenting the partitioning of a barnase (Ba) protein fused to a positively charged leading sequence ($pb_2$), $pb_2$-Ba, into the FhuA ΔC/Δ4L protein nanopore. At greater applied voltages, partitioning of a single $pb_2$-Ba protein into the nanopore interior was observed by a permanent single-channel current blockade. Both proteins are shown at the same scale. (b) Inspection of the interaction of the $pb_2$-Ba proteins with the FhuA ΔC/Δ4L protein nanopore produces a distinctive macroscopic current decay. The macroscopic currents were normalized to the value that corresponded to the initial time of each electrical trace. The chamber solution containing 20 mM KCl, 10 mM potassium phosphate, pH 7.4, 100 nM $pb_2$-Ba was added to the *trans* side of the chamber. The applied transmembrane potential was +80 mV. (c) Cartoon presenting the underlying sensing mechanism for the digestion of immunoglobulin G (IgG) by pepsin. The IgG partitioning into the nanopore interior was observed by short-lived, single-channel current blockades. (d) Time-dependent digestion of IgG by pepsin. 2.6 μM IgG was incubated with 1.5 units of pepsin in 25 μL of 1 M NaCl, phosphate-citrate buffer, pH 3.9. The reactions were quenched at the indicated times by the addition of 25 μL of 2 M Tris, pH 11.5. Samples were loaded and visualized as in Figure 1c. Bands were quantified using ImageJ software. (e) Nanopore-based assay for the digestion of IgG by pepsin. Representative 30-s durations of single-channel electrical traces of FhuA ΔC/Δ4L alone (trace 1) or in the presence of pepsin (trace 2) or IgG (trace 3) or IgG and pepsin (traces 4 and 5). The buffer conditions and pepsin and IgG concentrations were the same as in part d. Pepsin and IgG were added to the *trans* side of the chamber. The applied transmembrane potential was +40 mV. (f) Plot showing the event frequency monitored during the digestion activity of pepsin in part e. The event frequency was calculated using bins of 12-s duration. The inset magnifies the first 10 min of the same plot.


dx.doi.org/10.1021/ja3043646 | *J. Am. Chem. Soc.* 2012, 134, 9521–9531

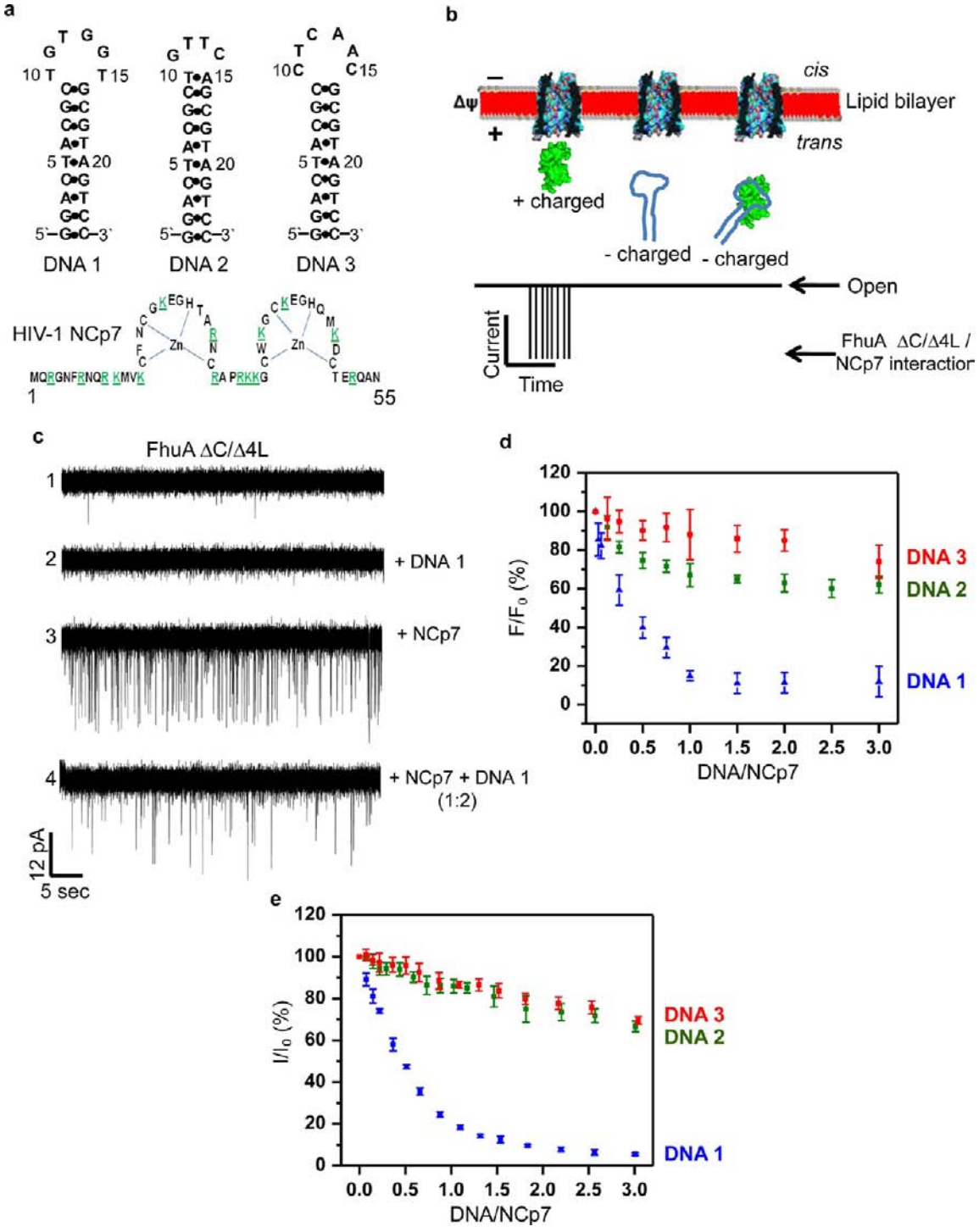


**Figure 5.** Probing the interactions of the NCp7 protein with a DNA aptamer using the FhuA ΔC/Δ4L protein nanopore. (a) The upper panel shows sequences of three DNA stem-loops. The bottom panel indicates the primary amino acid sequence of NCp7 from the pNL4-3 strain.[36] Positively charged amino acids are underlined and marked in green. The net charge of NCp7 at neutral pH is +9. (b) Cartoon presenting the principle for the detection of binding between NCp7 and DNA using the FhuA ΔC/Δ4L protein nanopore. The positively charged NCp7 interacts with the cation-selective FhuA ΔC/Δ4L nanopore as observed by transient single-channel current blockades. (c) Single-channel electrical recordings of FhuA ΔC/Δ4L alone (trace 1), FhuA ΔC/Δ4L in the presence of 2 $\mu$M DNA 1 aptamer (trace 2), FhuA ΔC/Δ4L in the presence of 1 $\mu$M NCp7 (trace 3), and FhuA ΔC/Δ4L in the presence of 1 $\mu$M NCp7 and 2 $\mu$M DNA 1 (trace 4). The reagents were added to the *trans* side of the chamber. The solution contained 5 mM sodium phosphate, 0.1% PEG, 0.2 M NaCl, 1 $\mu$M $ZnCl_2$, 1 mM tris(2 carboxyethyl) phosphine (TCEP), pH 7.0. The applied transmembrane potential was +40 mV. The electrical traces were low-pass Bessel filtered at 2 kHz. (d) Nanopore-probed titration assay of NCp7 with DNA 1, DNA 2, and DNA 3. The event frequencies were collected from 5-min-long single-channel current traces at each titration point; $F_0$ and $F$ are the frequencies before and after the addition of DNA, respectively. Other conditions for single-channel recordings were the same as in part c, except that different amount of DNA were added at each titration point. Each data point represents mean ± SD calculated from at least three distinct single-channel electrical recordings. (e) Fluorescence-probed titrations of NCp7 with DNA 1, 2, and 3. Buffer conditions were the same as in part c. The NCp7 concentration was 0.3 $\mu$M, and different amounts of DNA were added at each titration point. Each data point represents mean ± SD calculated from four distinct titration experiments.


dx.doi.org/10.1021/ja3043646 | *J. Am. Chem. Soc.* 2012, 134, 9521−9531

detection of the NCp7−DNA aptamer interaction is that the positively charged small NCp7 protein (+9) partitions into the cation-selective FhuA ΔC/Δ4L nanopore (Figure 5a, b). In contrast, DNA aptamers do not interact with the nanopore due to their strong negative charge (−23). When an NCp7 protein−DNA aptamer complex forms, the overall charge becomes negative and the overall size is greater. Therefore, the protein−nucleic acid complex likely does not interact with the nanopore (Figure 5b). The FhuA ΔC/Δ4L nanopore showed no significant current fluctuations in the binding buffer conditions (5 mM sodium phosphate, 0.1% PEG, 0.2 M NaCl, 1 $\mu$M $ZnCl_2$, 1 mM tris(2 carboxyethyl) phosphine (TCEP), pH 7.0) (Figure 5c, trace 1). The presence of the DNA 1 aptamer within the *trans* side of the chamber did not produce current blockades (Figure 5c, trace 2), but the addition of 1 $\mu$M NCp7 protein produced transient current blockades (Figure 5c, trace 3).

The frequency of the NCp7-produced current blockades decreased by ∼85% when 2 $\mu$M DNA 1, a high-affinity DNA aptamer (Supporting Information), was added to the *trans* side of the chamber (Figure 5c, trace 3). We interpret this finding as the formation of the NCp7-DNA 1 aptamer complex. If this is true, the current amplitude and the dwell time of the transient, NCp7-produced current blockades should not be altered after the addition of DNA 1 to the chamber. Indeed, these features were not changed by the addition of DNA 1 to the chamber (Supporting Information, Figure S12). Moreover, the dwell time was independent of the concentration of the DNA 1 aptamer (Supporting Information, Figure S12). The titration experiments were carried out with a molar ratio of DNA to NCp7 covering the range 0−3 (Figure 5d). Two other DNAs, DNA 2 and DNA 3 (Figure 5a), with different loop bases, were shown to have much lower binding affinity. Data fitting, assuming the stoichiometry of 1:1 for the DNA aptamer−NCp7 protein complex formation (Supporting Information), gave $K_d$ of 50 nM, 2.2 $\mu$M, and 8.8 $\mu$M for DNA 1, DNA 2, and DNA 3, respectively. Again, these experiments would be hard to achieve with $\alpha$HL, because of its intrinsic large-amplitude current blockades at physiological salt concentration (Figure 3a). Moreover, we were not able to distinguish the presence of the NCp7−DNA 1 complex in the aqueous phase using $\alpha$HL at an elevated salt concentration of 500 mM KCl, at which its intrinsic large-amplitude current blockades were absent (Supporting Information, Figure S13).[20]

We also executed fluorescence-monitored titrations of the interactions between NCp7 and DNA aptamers in the bulk aqueous phase (Supporting Information)[39] in parallel with these nanopore-based examinations, enabling the determination of the specificity of the different DNA stem-loops to NCp7 (Figure 5b). The absolute affinities of the DNAs in Figure 5a were determined by measuring the quenching of the single tryptophan in the NCp7 protein that is caused by stacking a loop G-base on Trp37.[36] NCp7 binds DNA 1 in a similar fashion to SL3 RNA from the HIV-1 packaging domain. The early points in the fluorescence titration of NCp7 with DNA 1 confirmed that the complex has a 1:1 stoichiometry (extrapolation to zero intensity at a molar ratio of 1:1 is expected for such a complex). Fitting the binding isotherm with an equation for the formation of a bimolecular complex[37] (Supporting Information) gave $K_d$ of 16 nM for the high-affinity DNA 1 aptamer, while $K_d$ values of 1.6 $\mu$M and 2.0 $\mu$M for DNA 2 and DNA3, respectively, were determined. Similar binding kinetics of the NCp7-nucleic acid complex, under the same conditions, were confirmed by isothermal titration calorimetry and surface plasmon resonance imaging.[39,40] The dissociation constants obtained from both assays are similar, reinforcing the reliability of the nanopore-based examinations of the kinetics of protein−DNA interactions at physiological salt concentration.

## 3. CONCLUSIONS

Obtaining a stiff and open redesigned $\beta$-barrel protein was not only a result of targeted deletion of its gating flexible parts of the lumen[41] but also an adaptation of the refolding protocol, thus producing a nanopore with superior stability of the open-state current under a wide range of conditions (Supporting Information, Figures S14 and S15). The robustness of FhuA ΔC/Δ4L at low salt concentration will ignite numerous explorations of biomolecular events under physiologically pertinent conditions. In addition, this trait will also permit the sensing of very weak binding events between an analyte and FhuA ΔC/Δ4L or among a complex of analytes, as weak interactions may be preserved under low-salt concentration conditions. Moreover, a rigid protein nanopore at a physiological salt concentration and at a highly acidic pH might be a suitable platform for exploring biomolecular events involved in toxin infection.[42] A pH-resistant protein nanopore shows prospects for further engineering to design customized nanovalves employed in drug-delivery carriers for acidic places of the body, such as the stomach.[43] Given the cross-sectional size of the nanopore lumen, with an average diameter greater than ∼2 nm and the quality of the signal-to-noise ratio, future applications might include the investigation of the translocation of double-stranded DNA through a protein nanopore and the interactions of DNA and RNA with a wide variety of interacting proteins. A robust protein nanopore at an elevated temperature might be instrumental in exploring the dissociation or unfolding events in nucleic acids, proteins, and their complexes. Since FhuA ΔC/Δ4L is a cation-selective $\beta$-barrel pore, an archetype of protein translocation in mitochondria, chloroplasts, and Gram-negative bacteria,[44] this engineered protein might also be employed as a model system for the examination of how a single polypeptide unfolds and traverses a transmembrane pore in a membrane.

One limitation of this engineered nanopore for its use in sensing technologies is the softness of the lipid membrane. To overcome this challenge, significant progress has recently been made in the implementation of a single protein nanopore within an artificial solid-state nanopore.[45] The monomeric structure of the engineered FhuA ΔC/Δ4L protein nanopore will enable a myriad of opportunities for direct genetic engineering without going through lengthy and laborious processes of preparation and purifications that are required for multimeric protein nanopores.[46] A satisfactory yield of the refolded FhuA ΔC/Δ4L protein nanopore makes it not only a reliable, versatile, and tractable model for fundamental explorations in membrane protein folding, structure, stability, and design but also a convenient platform for numerous application areas in medical bionanotechnology.

## ■ ASSOCIATED CONTENT

### Supporting Information

(i) Preparation of the *fhua Δc/Δ4L* gene, (ii) overexpression and purification of the FhuA ΔC/Δ4L protein under denaturing conditions, (iii) refolding of FhuA ΔC/Δ4L, (iv) electrical recordings on planar lipid bilayers, (v) preparation of barnase mutants, pepsin, and mouse serum immunoglobulin G (IgG) proteins and NCp7 protein, (vi) preparation of the DNA stem-loops; (vii) NCp7 titration assays, (viii) calculating the ionic selectivity of FhuA ΔC/Δ4L, (ix)


dx.doi.org/10.1021/ja3043646 | J. Am. Chem. Soc. 2012, 134, 9521−9531

comparison of the unitary conductance measured with FhuA ΔC/Δ4L refolded in different detergents, (x) insertion of the FhuA ΔC/Δ4L nanopore into the lipid bilayer in a single orientation, (xi) demonstration that the FhuA ΔC/Δ4L protein forms a rigid and unusually rigid protein nanopore under a broad range of conditions, (xii) comparison of channel closure rates between αHL and the engineered FhuA ΔC/Δ4L, (xiii) the *I*−*V* curves of the single-channel currents through the FhuA ΔC/Δ4L protein nanopores in symmetrical and asymmetrical solutions, (xiv) detection of modified proteins by the engineered FhuA ΔC/Δ4L protein nanopore, (xv) characteristics of protein analytes and their interactions with the FhuA ΔC/Δ4L protein nanopore, (xvi) digestion of immunoglobulin G (IgG) by pepsin, (xvii) exploration of the kinetics of Ncp7-DNA 1 interactions using the αHL nanopore, (xviii) sensitivity of membrane-extracted FhuA ΔC/Δ4L to low salt concentration or highly acidic pH, (xix) comparison between αHL and the engineered FhuA ΔC/Δ4L nanopores at low physiological salt concentration and highly acidic pH. This material is available free of charge via the Internet at http://pubs.acs.org.

## AUTHOR INFORMATION


### Corresponding Author

lmovilea@physics.syr.edu


### Notes

The authors declare no competing financial interest.

## ACKNOWLEDGMENTS

We thank Andreas Matouschek for the generous gift of $pb_2$-Ba plasmids, and Stewart Loh and Bert van den Berg for constructive comments on the manuscript. We are also grateful to David J. Niedzwiecki for single-channel experiments with dextran and to Tatyana Konyakhina for electrophysiology data with αHL and the NCp7 aptamers. This work was funded by the U.S. National Science Foundation Grants DMR-1006332 (L.M.) and DGE-1068780 (IGERT Program), and the National Institutes of Health grants R01 GM088403 (L.M.), R01 GM032691 (P.N.B.), and R44 GM076811 (M.P.M.).

## REFERENCES


(1) Braun, T.; Ghatkesar, M. K.; Backmann, N.; Grange, W.; Boulanger, P.; Letellier, L.; Lang, H. P.; Bietsch, A.; Gerber, C.; Hegner, M. *Nat. Nanotechnol.* **2009**, *4* (3), 179−185.

(2) Bayley, H.; Martin, C. R. *Chem. Rev.* **2000**, *100* (7), 2575−2594.

(3) Bayley, H.; Cremer, P. S. *Nature* **2001**, *413* (6852), 226−230.

(4) Branton, D.; Deamer, D. W.; Marziali, A.; Bayley, H.; Benner, S. A.; Butler, T.; Di Ventra, M.; Garaj, S.; Hibbs, A.; Huang, X.; Jovanovich, S. B.; Krstic, P. S.; Lindsay, S.; Ling, X. S.; Mastrangelo, C. H.; Meller, A.; Oliver, J. S.; Pershin, Y. V.; Ramsey, J. M.; Riehn, R.; Soni, G. V.; Tabard-Cossa, V.; Wanunu, M.; Wiggin, M.; Schloss, J. A. *Nat. Biotechnol.* **2008**, *26* (10), 1146−1153.

(5) Movileanu, L. *Trends Biotechnol.* **2009**, *27* (6), 333−341.

(6) Majd, S.; Yusko, E. C.; Billeh, Y. N.; Macrae, M. X.; Yang, J.; Mayer, M. *Curr. Opin. Biotechnol.* **2010**, *21* (4), 439−476.

(7) Shin, S. H.; Luchian, T.; Cheley, S.; Braha, O.; Bayley, H. *Angew. Chem., Int. Ed. Engl.* **2002**, *41* (19), 3707−3709.

(8) Ferguson, A. D.; Hofmann, E.; Coulton, J. W.; Diederichs, K.; Welte, W. *Science* **1998**, *282* (5397), 2215−2220.

(9) Locher, K. P.; Rees, B.; Koebnik, R.; Mitschler, A.; Moulinier, L.; Rosenbusch, J. P.; Moras, D. *Cell* **1998**, *95* (6), 771−778.

(10) Pawelek, P. D.; Croteau, N.; Ng-Thow-Hing, C.; Khursigara, C. M.; Moiseeva, N.; Allaire, M.; Coulton, J. W. *Science* **2006**, *312* (5778), 1399−1402.

(11) Ferguson, A. D.; Braun, V.; Fiedler, H. P.; Coulton, J. W.; Diederichs, K.; Welte, W. *Protein Sci.* **2000**, *9* (5), 956−963.

(12) Ferguson, A. D.; Kodding, J.; Walker, G.; Bos, C.; Coulton, J. W.; Diederichs, K.; Braun, V.; Welte, W. *Structure* **2001**, *9* (8), 707−716.

(13) Braun, V. *J. Bacteriol.* **2009**, *191* (11), 3431−3436.

(14) Killmann, H.; Benz, R.; Braun, V. *J. Bacteriol.* **1996**, *178* (23), 6913−6920.

(15) Braun, M.; Killmann, H.; Maier, E.; Benz, R.; Braun, V. *Eur. J. Biochem.* **2002**, *269* (20), 4948−4959.

(16) Mohammad, M. M.; Howard, K. R.; Movileanu, L. *J. Biol. Chem.* **2011**, *286* (10), 8000−8013.

(17) Kleinschmidt, J. H.; Tamm, L. K. *Biochemistry* **1999**, *38* (16), 4996−5005.

(18) Burgess, N. K.; Dao, T. P.; Stanley, A. M.; Fleming, K. G. *J. Biol. Chem.* **2008**, *283* (39), 26748−26758.

(19) Bezrukov, S. M.; Vodyanoy, I. *Biophys. J.* **1993**, *64* (1), 16−25.

(20) Mohammad, M. M.; Movileanu, L. *J. Phys. Chem. B* **2010**, *114* (26), 8750−8759.

(21) Howorka, S.; Siwy, Z. *Chem. Soc. Rev.* **2009**, *38* (8), 2360−2384.

(22) Olasagasti, F.; Lieberman, K. R.; Benner, S.; Cherf, G. M.; Dahl, J. M.; Deamer, D. W.; Akeson, M. *Nat. Nanotechnol.* **2010**, *5* (11), 798−806.

(23) Wang, Y.; Zheng, D.; Tan, Q.; Wang, M. X.; Gu, L. Q. *Nat. Nanotechnol.* **2011**, *6* (10), 668−674.

(24) Butler, T. Z.; Pavlenok, M.; Derrington, I.; Niederweis, M.; Gundlach, J. H. *Proc. Natl. Acad. Sci. U. S. A* **2008**, *105* (52), 20647−20652.

(25) Derrington, I. M.; Butler, T. Z.; Collins, M. D.; Manrao, E.; Pavlenok, M.; Niederweis, M.; Gundlach, J. H. *Proc. Natl. Acad. Sci. U. S. A* **2010**, *107* (37), 16060−16065.

(26) Wendell, D.; Jing, P.; Geng, J.; Subramaniam, V.; Lee, T. J.; Montemagno, C.; Guo, P. *Nat. Nanotechnol.* **2009**, *4* (11), 765−772.

(27) Korchev, Y. E.; Bashford, C. L.; Alder, G. M.; Kasianowicz, J. J.; Pasternak, C. A. *J. Membr. Biol.* **1995**, *147* (3), 233−239.

(28) Kasianowicz, J. J.; Bezrukov, S. M. *Biophys. J.* **1995**, *69* (1), 94−105.

(29) Maglia, G.; Henricus, M.; Wyss, R.; Li, Q.; Cheley, S.; Bayley, H. *Nano Lett.* **2009**, *9* (11), 3831−3836.

(30) Kang, X. F.; Gu, L. Q.; Cheley, S.; Bayley, H. *Angew. Chem., Int. Ed. Engl.* **2005**, *44* (10), 1495−1499.

(31) Huang, S.; Ratliff, K. S.; Matouschek, A. *Nat. Struct. Biol.* **2002**, *9* (4), 301−307.

(32) Mohammad, M. M.; Prakash, S.; Matouschek, A.; Movileanu, L. *J. Am. Chem. Soc.* **2008**, *130* (12), 4081−4088.

(33) Zhao, Q.; de Zoysa, R. S.; Wang, D.; Jayawardhana, D. A.; Guan, X. *J. Am. Chem. Soc.* **2009**, *131* (18), 6324−6325.

(34) Jones, R. G.; Landon, J. *J. Immunol. Methods* **2002**, *263* (1−2), 57−74.

(35) Linial, M. L.; Miller, A. D. *Curr. Top. Microbiol. Immunol.* **1990**, *157*, 125−152.

(36) De Guzman, R. N.; Wu, Z. R.; Stalling, C. C.; Pappalardo, L.; Borer, P. N.; Summers, M. F. *Science* **1998**, *279* (5349), 384−388.

(37) Paoletti, A. C.; Shubsda, M. F.; Hudson, B. S.; Borer, P. N. *Biochemistry* **2002**, *41* (51), 15423−15428.

(38) Shubsda, M. F.; Paoletti, A. C.; Hudson, B. S.; Borer, P. N. *Biochemistry* **2002**, *41* (16), 5276−5282.

(39) Athavale, S. S.; Ouyang, W.; McPike, M. P.; Hudson, B. S.; Borer, P. N. *Biochemistry* **2010**, *49* (17), 3525−3533.

(40) Athavale, S. S. Ph.D. Thesis. Syracuse University, Syracuse, NY, 2010.

(41) Chen, M.; Khalid, S.; Sansom, M. S.; Bayley, H. *Proc. Natl. Acad. Sci. U. S. A* **2008**, *105* (17), 6272−6277.

(42) Krantz, B. A.; Melnyk, R. A.; Zhang, S.; Juris, S. J.; Lacy, D. B.; Wu, Z.; Finkelstein, A.; Collier, R. J. *Science* **2005**, *309* (5735), 777–781.
(43) Langer, R. *Nature* **1998**, *392* (6679 Suppl), 5–10.
(44) Wickner, W.; Schekman, R. *Science* **2005**, *310* (5753), 1452–1456.
(45) Hall, A. R.; Scott, A.; Rotem, D.; Mehta, K. K.; Bayley, H.; Dekker, C. *Nat. Nanotechnol.* **2010**, *5* (12), 874–877.
(46) Braha, O.; Walker, B.; Cheley, S.; Kasianowicz, J. J.; Song, L. Z.; Gouaux, J. E.; Bayley, H. *Chem. Biol.* **1997**, *4* (7), 497–505.